Exploiting Path Diversity in Datacenters using MPTCP-aware SDN

Tomas Urban and Martin Oravsky

Faculty of Informatics and Information Technologies, Slovak Technical University

Recently, Multipath TCP (MPTCP) has been proposed as an alternative transport approach for datacenter networks. MPTCP provides the ability to split a flow into multiple paths thus providing better performance and resilience to failures. Usually, MPTCP is combined with flow-based EqualCost Multi-Path Routing (ECMP), which uses random hashing to split the MPTCP subflows over different paths. However, random hashing can be suboptimal as distinct subflows may end up using the same paths, while other available paths remain unutilized. In this paper, we explore an MPTCP-aware SDN controller that facilitates an alternative routing mechanism for the MPTCP subflows. The controller uses packet inspection to provide deterministic subflow assignment to paths. Using the controller, we show that MPTCP can deliver significantly improved performance when connections are not limited by the access links of hosts. To lessen the effect of throughput limitation due to access links, we also investigate the usage of multiple interfaces at the hosts. We demonstrate, using our modification of the MPTCP Linux Kernel, that using multiple subflows per pair of IP addresses can yield improved performance in multi-interface settings.

1. INTRODUCTION

The Transmission Control Protocol (TCP) is used by the vast majority of applications to transport their data reliably across the Internet. TCP was designed in the 1970s, and neither mobile devices nor computers with many network interfaces were an immediate design priority. On the other hand, the TCP designers knew that network links could fail, and they chose to decouple the network-layer protocols (Internet Protocol) from those of the transport layer (TCP) so that the network could reroute packets around failures without affecting TCP connections. This ability to reroute packets is largely due to the use of dynamic routing protocols, and their job is made much easier because they dont need to know anything about transport-layer connections.

Todays networks can be multipath: mobile devices have multiple wireless interfaces, datacenters have many redundant paths between servers, and multihoming has become the norm for big server farms. Meanwhile, TCP is essentially a single-path protocol: when a TCP connection is established, the connection is bound to the IP addresses of the two communicating hosts. If one of these addresses changes, for whatever reason, the connection will fail. In fact, a TCP connection cannot even be load balanced across more than one path within the network, because this results in packet reordering, and TCP misinterprets this reordering as congestion and slows down.

This mismatch between todays multipath networks and TCPs single-path design creates tangible problems. For instance, if a smartphones WiFi loses signal, the TCP connections associated with it stall; there is no way to migrate them to other working interfaces, such as 3G. This makes mobility a frustrating experience for users. Modern datacenters are another example: many paths are available between two endpoints, and multipath routing randomly picks one for a particular TCP connection. This can cause collisions where multiple flows get placed on the same link, thus hurting throughput to such an extent that average throughput is halved in some scenarios.

Multipath TCP (MPTCP)[A. Ford and C. Raiciu and M. Handley and O. Bonaventure year] [Raiciu et al. 2012] is a major modification to TCP that allows multiple paths to be used simultaneously by a single transport connection. Multipath TCP circumvents the issues mentioned above and several others that affect TCP. Changing TCP to use multiple paths is not a new idea; it was originally proposed more than 15 years ago by Christian Huitema in the Internet Engineering Task Force (IETF), and there have been a half-dozen more proposals since then to similar effect. Multipath TCP draws on the experience gathered in previous work, and goes further to solve issues of fairness when competing with regular TCP and deployment issues as a result of middleboxes in todays Internet. The Multipath TCP protocol has recently been standardized by the IETF, and an implementation in the Linux kernel is available today[C. Paasch and S. Barre and J. Korkeaniemi and F. Duchene and G. Detal year].

2.   ANALYSIS

2.1   Chapter introduction

This chapter is a brief analysis of Software defined networking and how it can benefit from multipath transmission control protocols, especially in datacenter-like topologies by exploiting path diversity.

In chapter 2.2, the basic concept of software defined networking will be introduced. Chapter 2.3 will briefly talk about Multipath TCP protocol which will be used later in this document. Chapter 2.4 will consider several problems regarding poor performance of SDNs due to random path selection.

2.2   Software defined networking

Todays networks mainly consist of routers, switches, hosts and many other network devices. In order for hosts to communicate, routers and switches performs as a transfer point between source and destination. These devices must provide very fast and reliable transfer of information, which, since the need for fast Internet connection is bigger and bigger every year, can be challenging.

The basic network device consists of data plane and control plane. Data plane is responsible for receiving the incoming packet and forwarding it to devices control plane, where the packet is processed. Control plane then forwards the packet again to the data plane, which then sends the packet via correct outgoing interface. This causes network device to store a lot of information and the CPU load can become quite high.

Software defined networking is an architectural approach that optimizes and simplifies network operation by more closely binding the interaction (i.e., provosioning, messaging and alarming) among applications and network services and devices, whether they be real or virtualized. [Nadeau and Gray 2013]

SDNs use centralized object known as controller, which does all the computing and routing of the communication. The controller installs various forwarding rules based on global view of network topology on forwarders. Forwarders (also known as switches) are simple devices which forward the communication based on the rules installed by controller. If packet arrives on forwarder interface and no rule is matched, forwarder sends the packet to controller using OpenFlow protocol. The controller then processes the packet (e.g. flooding ARP request) and sends the packet back to forwarders along with corresponding rule.

This enables the network to better handle the communication while using the hardware resources better.

2.3   Multipath TCP

There are several options when sending communication on multiple path simultaneously while providing better redundancy and throughput. One can use Stream control transmission protocol (SCTP) which uses the concept of streams. When there is a need for L2 redundancy, bonding has proven itself as a good alternative.

In this document we propose Multipath TCP as a great alternative for improving path diversity in multipath communication in datacenter-like topologies.

Multipath TCP utilizes one TCP connection on multiple paths, on which separate TCP subflows are created, thus providing improved throughput and redundancy. Multipath TCP eliminates single point of failure by ability to switch communication to a working path when another path goes down. Multipath TCP enabled hosts use Multipath TCP options to establish a connection or to add a new subflow to an existing connection.

2.4   Problems with Multipath TCP and SDNs

Software defined networking can greatly benefit from Multipath TCP capabilities. However, software defined networks do not handle MPTCP traffic differently than the classic single-path TCP traffic. In order to exploit path diversity better and to provide true redundancy to the network, further implementation on the controller is necessary.

A key aspect that affects MPTCP performance is the routing mechanism of the subflows. Currently, the most prominent and widely deployed routing mechanism in datacenters is a flow-based variant of Equal-Cost Multi-Path Routing (ECMP) [2]. However, ECMP uses random hashing to split the subflows over different paths. This can cause a variety of problems, from which the most important is the high probability that multiple subflows end up on the same path while other paths remain not utilized properly. This also destroys the idea of redundancy.

The number of subflows is also a crucial aspect to performance of the network. Although the idea of more subflows can mean faster networks, the more subflows MPTCP use, the bigger the overhead is. More subflows mean more rules installed in forwarders and higher CPU utilization for the controller.

As shown in previous papers, MPTCP throughput also correlates with number of used interfaces on hosts. We will also deal with this issue since one-homed devices can quickly become a bottleneck in this type of network.

The purpose of this assessment is to implement an intelligent routing protocol that makes software defined networks MPTCP-aware by exploiting path diversity.

3.   RELATED WORK IN COMPUTER GRAPHICS

A few researchers have addressed the issue of realistic human iris synthesis. Lefohn et al. blend several textures created by an artist, each containing some eye feature. Other image-based approaches have been proposed by Cui et al., Wecker et al., and Makthal and Ross. Essentially, they decompose a set of iris images using techniques such as principal component analysis, multiresolution and wavelets, and Markov random fields, and recombine the obtained data to generate new images of irises. Zuo and Schmid created a fiber-based 3D model of the iris. Lam and Baranoski introduced a predictive light transport model for the human iris, which computes the spectral responses of iridal tissues described by biophysical parameters. François et al. estimate iris height maps from gray-scale images. All these approaches use stationary pupil sizes.

Sagar et al. developed an anatomically detailed model of the eye to be used in a surgical simulator. In their model, Gaussian perturbations were used to simulate the waviness of ciliary fibers and the retraction of pupillary fibers during pupil dilation. Alternatively, depending on the level of object manipulation, a texture mapping approach was used to model the iridal appearance. It is worth noting, however, that their goal was to achieve functional realism [DeCarlo and Santella 2002] as opposed to physical or photorealism.

4.   BRIEF OVERVIEW OF THE HUMAN IRIS AND PUPIL

The human iris has a diameter of about 12 mm and forms a disc that controls how much light reaches the retina. Under high levels of lighting, the iris dilates, flattening itself and decreasing the pupil size. Under low levels of illumination, it constricts, folding itself and increasing the pupil area. The pupil diameter varies from 1.5 mm to 8 mm on average, and in general, it is not a perfect cir-

cle. Also, its center may deviate from the center of the iris by an offset of up to 20%. According to Newsome and Loewenfeld, there are no observable differences in the iris regarding light-induced or drug-induced pupil dilation/constriction.

The human iris is divided in two zones by the *collarette*, a delicate zig-zag line also known as the iris frill. The *pupillary* zone is bounded by the pupil, while the *ciliary* zone extends to the outer border of the iris. Each zone is characterized by a muscle. The *sphincter*, located in the pupillary zone, is a concentric muscle that constricts to decrease the pupil size. The *dilator*, found in the ciliary zone, is a radial muscle that constricts to increase the pupil size. These two muscles overlap at the collarette.

The sphincter and dilator muscles are independently connected to the autonomous nervous system (ANS) and the pupil size results from a balance of the separately incoming stimuli to the two muscles [Dodge 1900]. The ANS conducts the pupillary light reflex and *hippus* neural actions. Hippus are spontaneously irregular variations in pupil diameter, which can essentially be characterized as random noise in the 0.05 to 0.3 Hz frequency range. In PLR, when light reaches the retina, neural signals are sent to the brain, which sends back a signal for closing or opening the pupil. Thus, PLR can be modeled in two phases: perception, and after some time delay, adjustment.

5. MODELS OF PUPIL DYNAMICS

The pupillometry literature describes several models built around experiments designed to measure the values of some parameters as a function of incident light intensity. Link and Stark performed a study where a light source was placed in front of the subjects' irises and, by varying the intensity and frequency of the light, they measured the pupillary latency (the time delay between the instant in which the light pulse reaches the retina and the beginning of iridal reaction):

$$\tau(R, L_{fL}) = 253 - 14\,ln(L_{fL}) + 70R - 29\,R\,ln(L_{fL}), \quad (1)$$

where τ is the latency in milliseconds, L_{fL} is the luminance measured in foot-Lamberts (fL), and R is the light frequency measured in Hz.

Other similar models predict an average pupil size as a function of the light intensity using a few experimental measurements [Dodge and Cline 1901]. Among those, the most popular one is the Moon and Spencer model, which is expressed as:

$$D = 4.9 - 3\,tanh[0.4(log_{10}(L_b) - 0.5)], \quad (2)$$

where the pupil diameter, D, varies from 2 to 8 mm, and L_b is the background luminance level expressed in blondels, varying from 10^5 blondels in sunny days to 10^{-5} blondels in dark nights. $tanh$ is the hyperbolic tangent.

5.1 Physiologically-Based Models

In Mathematical Biology and related fields, models based on physiological and anatomical observations were derived to express the relationships among the pupillary action variables without relying on quantitative experimental data. For example, Usui and Stark proposed a parametric model of the iris to describe the static characteristics of pupil response to light stimuli, and to explain its random fluctuations in terms of probability density functions. Recently, Tilmant et al. proposed a model of PLR based on physiological knowledge and guided by experiments. Although they have obtained plausible results, Tilmant et al. have recommended the use of another physiologically-based model to more accurately monitor

pupillary dynamics, namely the time-dependent model developed by Longtin and Milton.

Longtin and Milton define the efferent neural signal $E(t)$ arriving at the iris per unit of time t, as:

$$E(t) = \beta\,ln\left[\frac{\phi(t-\tau)}{\bar{\phi}}\right], \quad (3)$$

where β is a constant of proportionality and ϕ is the retinal light flux measured in lumens and defined by Stark and Sherman as $\phi = I_l A$: illuminance (I_l, in lumens/mm^2) times the pupil area (A, in mm^2). τ is the latency, and $\bar{\phi}$ is the retinal light level threshold (the light level below which there is no change in the pupil area). The notation $\phi(t-\tau)$ indicates that the current effect depends on the retinal light flux at a time τ milliseconds in the past. As the efferent neural signal reaches the iris, it induces some muscular activity x that may cause the pupil to dilate or constrict. According to Partridge and Benton, the relationship between $E(t)$ and x can be approximated by:

$$E(t) \tilde{=} k\left(\frac{dx}{dt} + \alpha x\right), \quad (4)$$

where k is a proportionality factor and α is a rate constant that depends on the definition and units of x used in the model. Longtin and Milton combine Equations (3) and (4) as:

$$\frac{dx}{dt} + \alpha x = \gamma\,ln\left[\frac{\phi(t-\tau)}{\bar{\phi}}\right]. \quad (5)$$

They express the pupil area as $A = f(x)$ and use the inverse $f^{-1}(A) = g(A) = x$ to remove x from Equation (5). In their paper, Longtin and Milton use a Hill function [Duchowski 2002] (Equation 6) as the function f, since it can approximate the elasto-mechanical properties of the iris during the pupillary activity:

$$A = f(x) = \frac{\Lambda\theta^n}{\theta^n + x^n} + \Lambda'. \quad (6)$$

Here, Λ' and $\Lambda + \Lambda'$ are, respectively, the minimum and the maximum pupil areas, and θ is the value of x corresponding to the average pupil area. Longtin and Milton's model then becomes:

$$\frac{dg}{dA}\frac{dA}{dt} + \alpha g(A) = \gamma\,ln\left[\frac{\phi(t-\tau)}{\bar{\phi}}\right], \quad (7)$$

where

$$g(A) = x = \sqrt[n]{\frac{\Lambda\theta^n}{A - \Lambda'} - \theta^n}. \quad (8)$$

An S-shaped curve similar to the Hill function has been described in the physiologically-based model of Usui and Stark to approximate the pupil diameter of an average individual under static illumination conditions.

6. THE PROPOSED PHYSIOLOGICAL-BASED MODEL

The model of Moon and Spencer (Equation (2)) is based on a set of discrete measurements and approximates the response on an average individual under various lighting conditions. Their measurements were made after the pupil size had stabilized for each illumination level, and therefore, their model does not describe the pupil behavior outside the equilibrium state. Moreover, pupil size, latency, constriction, and redilation velocities tend to vary among

individuals exposed to the same lighting stimulus [Gajewski et al. 2005]. We remark that such variations are not captured by the model of Moon and Spencer.

Longtin and Milton's model (Equation (7)) is time dependent and adaptive, with the potential to handle abrupt lighting changes. It is a theoretical model, and unfortunately, Longtin and Milton did not provide the values for the various parameters in their model (*i.e.*, γ, α, θ, n, $\bar{\phi}$), as these, in principle, depend on the abstract notion of iridal muscular activity x, as well as on the use of the Hill function. The use of incorrect parameter values will not produce realistic results and may cause Equation (7) to not converge.

Starting from Longtin and Milton's and from Moon and Spencer's models, we derive a practical model that predicts the pupil diameter for the nonequilibrium case based on experimental data (Section 6.2). In Section 6.3, we show how we can extend this basic model to take individual variability into account.

6.1 Equilibrium Case

Under constant lighting conditions, the pupil area in Longtin and Milton's model will converge to an equilibrium state, where:

$$\frac{dg}{dA}\frac{dA}{dt} = 0.$$

Under such a circumstance, and assuming there is no occurrence of hippus, ϕ becomes time invariant. Also, recall that $ln(m/n) = ln(m) - ln(n)$, and therefore, one can rewrite Longtin and Milton's model (Equation (7)) for the equilibrium case as:

$$\alpha g(A) = \gamma \left(ln(\phi) - ln(\bar{\phi}) \right). \quad (9)$$

In turn, the Moon and Spencer model can be rewritten as

$$\left(\frac{D - 4.9}{3} \right) = \left[0.4 \left(\frac{ln}{(L_b)} ln(10) - 0.5 \left(\frac{ln}{(10)} ln(10) \right) \right) \right],$$

and since the hyperbolic tangent is an odd function, we can rewrite this equation as:

$$-2.3026 \, atanh \left(\frac{D - 4.9}{3} \right) = 0.4(ln(L_b) - 1.1513), \quad (10)$$

where $atanh$ is the arc-hyperbolic tangent. Comparing Equations (9) and (10), in order for Longtin and Milton's model to fit the response of Moon and Spencer's average subject under equilibrium conditions, one has:

$$-2.3026 \, atanh \left(\frac{D - 4.9}{3} \right) \approx \alpha g(A) \quad (11)$$

$$0.4(ln(L_b) - 1.1513) \approx \gamma(ln(\phi) - ln(\bar{\phi})). \quad (12)$$

From Equation (12) we can estimate the value of the parameter γ. One should note that L_b is expressed in blondels while ϕ is given in lumens. Although, in general one cannot convert between two photometric quantities, this can be done under some well-defined situations. Since Moon and Spencer's data were collected with the subject seated before a large white screen of uniform intensity which covers most of their field of view, we assume that the light reaching a person's pupil has been reflected by a perfect (Lambertian) diffuse surface. Recall that an ideal (lossless) diffuse reflector returns all of the incident flux so that its reflectance $\rho = 1$ and its BRDF $f = 1/\pi$. For such a reflector, 1 blondel $= 10^{-6}$ lumens/mm^2.

Since the light flux, ϕ, depends on the area of the pupil, in order to estimate γ, we first evaluate the left-hand side of Equation (12) for the entire range of illumination covered by Moon and Spencer's model: $L_b \in \left[10^{-5}, 10^5 \right]$ blondels. For each value of
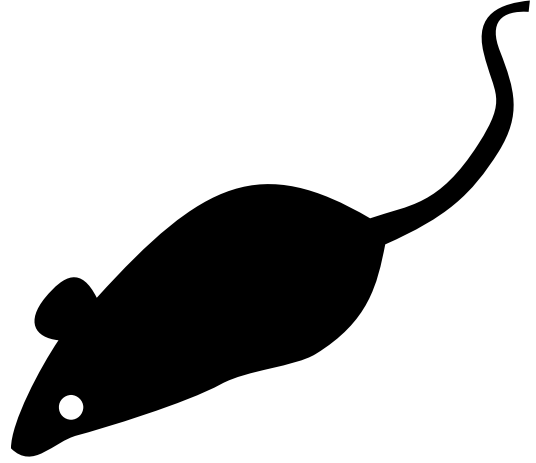
Fig. 1. High-quality fittings: (left) Both sides of Equation 13. (right) Equations 2 and 15, whose difference in absolute values is under 2% over the entire range $[10^{-5}, 10^5]$ blondels.

L_b, we then use Equation (2) to estimate D, from which the pupil area $A = \pi(D/2)^2$, and then ϕ, are computed. The retinal light level threshold $\bar{\phi} = 4.8118 \times 10^{-10}$ lumens was obtained using the pupil diameter $D_t = 7.8272$ mm, predicted by Equation 2 for $L_b = 10^{-5}$ blondels ($\bar{\phi} = \pi(7.8272/2)^2 \ mm^2 \times 10^{-5}10^{-6}$ lumens/mm^2). Using the tabulated data for the left-hand side of Equation (12) and the conversion scheme just described, we get the following fitting:

$$0.4(ln(L_b) - 1.1513) \approx 0.45 \left(ln(\phi) - ln(\bar{\phi}) \right) - 5.2, \quad (13)$$

whose quality of approximation is illustrated in Figure 1 (left). The vertical axis of the graph (scaled muscular activity) represents $\alpha g(A)$, where $g(A) = x$ is the muscular activity. The extra constant -5.2 translates the function on the right-hand side of Equation 12 vertically, improving the fitting. Given Equation (13), we can replace $g(A)$ with $M(D)$ (Equation (11)), with $\alpha = -2.3026$, where $M(D)$ is given by:

$$M(D) = atanh \left(\frac{D - 4.9}{3} \right). \quad (14)$$

Thus, the equilibrium situation can be expressed by Equation (15). As expected, it approximates Moon and Spencer's function (Equation (2)) for the pupil diameter of the average subject quite well. The absolute value of the difference between Equations (2) and (15) is under 2% over the entire range of $[10^{-5}, 10^5]$ blondels (Figure 1 right).

$$2.3026 \, M(D) = 5.2 - 0.45 \, ln \left[\frac{\phi}{\bar{\phi}} \right] \quad (15)$$

6.2 The Dynamic Case

Equation (15) cannot be used to describe the evolution of the pupil diameter in time as a function of instantaneous variations of the light intensity arriving at the pupil. Nevertheless, the obtained constants are still valid for the dynamic case, since the equilibrium is just a special case of the more general pupil behavior, for which the constants should also hold.

In general, one cannot take an equation obtained for equilibrium and generalize it to the dynamic case. In our model, however, this is possible because of the following constraints:

(1) $g(A)$ and $M(D)$ have no explicit time dependence;
(2) the range of values assumed by A (or D) is the same for both the equilibrium and the nonequilibrium cases;
(3) there is a one-to-one mapping between A and D.

By introducing time in Equation (15), we obtain a delay differential equation that corresponds to our solution for the dynamic case:

$$dt_c = \frac{T_c - T_p}{S} \quad dt_d = \frac{T_c - T_p}{3S}, \qquad (16)$$

where T_c and T_p are respectively the current and previous simulation times (times since the simulation started) measured in milliseconds, S is a constant that affects the constriction/dilation velocity and varies among individuals. The higher the S value, the smaller the time step used in the simulation and, consequently, the smaller the pupil constriction/dilation velocity.

Figure 4 shows pupil diameter values corresponding to Moon and Spencer's average subject simulated using Equation (16) considering some abrupt changes in the environment luminance. For this example, our results are compared to results provided by the static models of Moon and Spencer (Equation (2)) and of De Groot and Gebhard.

6.3 Modeling Individual Differences

While Equation (16) simulates dynamic pupil behavior, it only does so for the average individual represented by the Moon and Spencer model. There are, however, substantial differences in the way pupils from different individuals react to a given light stimulus. Such variations include differences in diameter [Google Inc. year], latency, and constriction and redilation velocities. In order to simulate individual differences, we cannot just arbitrarily change the parameter values of our model, as Equation (16) may not converge.

Figure 3 shows the original data used by Moon and Spencer. The curve C_m (shown in black), was obtained by converting the values of L_b in the range of $[10^{-5}, 10^5]$ blondels to lumens (see Section 6.1) and then using Equation (15) to compute the corresponding pupil diameter values used for plotting. The top and bottom curves, C_t and C_b, respectively, define an envelope containing all pupil diameter values used by Moon and Spencer. C_b was obtained by fitting a 5 degree polynomial to 11 of the smallest pupil diameter values along the entire luminance range. Likewise, C_t was obtained by fitting a 5 degree polynomial to 11 of the largest pupil diameter values. We treat C_b, C_m, and C_t as isocurves $C(p)$ for some parameter $p \in [0, 1]$, so that $C(0) = C_b$, and $C(1) = C_t$. We then model individual differences by associating to each individual I, an index $r_I \in [0, 1]$, which corresponds to an isocurve, $C(r_I)$. This index can be randomly generated or, alternatively, it can be recovered from experimental data as described in Section 6.4. To avoid convergence problems and still achieve the results corresponding to isocurve $C(r_I)$, we rewrite C_t and C_b, respectively, as new functions C_{tD} and C_{bD} of the pupil diameter:

$$\begin{aligned} C_{tD}(D) = &-0.013D^5 + 0.322D^4 - 3.096D^3 \\ &+ 13.655D^2 - 25.347D + 18.179 \end{aligned} \qquad (17)$$

$$\begin{aligned} C_{bD}(D) = &-5.442D^5 + 1.387D^4 - 1.343D^3 \\ &+ 6.219D^2 - 1.317D + 1.219. \end{aligned} \qquad (18)$$

In order to obtain C_{tD}, we evaluate the functions C_m and C_t for L_b in the range $[10^{-5}, 10^5]$ blondels, creating ordered pairs of

diameter values $(D_m, D_t) = (C_m(L_b), C_t(L_b))$. Given enough of these pairs, we fit a curve expressing D_t as a function of D_m (or D for short). The resulting curve is C_{tD} (Equation (17)). The case of C_{bD} is similar. The final pupil diameter at any time is then obtained solving Equation 16 for D and then evaluating:

$$D_{final} = C_{bD}(D) + (C_{tD}(D) - C_{bD}(D))r_I. \qquad (19)$$

We have adopted this solution due to its simplicity and generality: we can easily replace the curves $C_{bD}(D)$ and $C_{tD}(D)$ with new ones, covering new data as they become available, or representing other models (e.g., De Groot and Gebhard). Since the relative distances of C_m to C_b and C_t vary for different values of D, no value of r_I will exactly recover C_m. This is not a problem, however, as C_m corresponds to the average subject. Other parameterizations are possible, including ones that interpolate C_m for a given value of r_I.

Although our model properly simulates the elastic behavior of the iris muscular activity during changes in lighting conditions, it does not model hippus (Equation 16 will converge to some pupil diameter value if the lighting conditions remain constant). As random fluctuations whose causes are still unknown, it is currently not possible to define a physiologically-based model for hippus. We visually approximate the hippus effect by adding small random variations to the light intensity (between $-10^{0.3}$ and $10^{0.3}$ blondels), to induce small variations in the pupil diameter (of the order of 0.2 mm), in the frequency range of 0.05Hz to 0.3Hz. This significantly improves the realism of the resulting simulations and animations. According to Usui and Stark, the standard deviation of the noise corresponds to approximately 10% of the pupil diameter.

6.4 The PLR Model Validation

In order to validate our PLR model under nonequilibrium conditions and to show that it is capable of representing individual variability, we performed some qualitative comparisons between actual pupil behavior and the results of simulations produced by our model. For this, we captured videos of normal subjects presenting significantly different light sensitivities (different PLR responses), while a light was turned on and off several times. Since pupil constriction is bigger when both eyes are stimulated, the subjects kept both eyes opened. To avoid fatigue and habituation of the iris, in each experiment we recorded less than one minute of video per subject.

—The image texel size of surface textures that represent 3D elements (e.g. forest) should vary with distance, but should not match true perspective (*texel size* in Section 3.2, Texture Gradients).
—The image space distribution of texel elements of 3D textures (e.g. forest) should mimic one that would result from the projection of homogeneously distributed surface elements (*texel density* in Section 3.2, Texture Gradients).
—Image space texel spacing of 3D textures should ensure that texels overlap, especially in steep areas (*texel occlusion* in Section 3.2, Texture Gradients).
—Fall lines follow essential structures of terrain. They act as surface contours, and are used by panorama artists to paint cliff and snow textures (*fall lines* in Section 3.2, Surface Contours).
—Fall lines are used as imaginary lines along which tree strokes are placed, acting as texture *meta-strokes* (*meta-strokes* in Section 3.2, Surface Contours).
—Shading tone should have a good distribution of light, medium, and dark values (*shading* in Section 3.2, Shading).

—Light position should be placed so that the rendering of the terrain exhibits a good balance of light and shade, as seen from the selected viewpoint (*light direction* in Section 3.2, Shading).

—For extended terrain areas, indicating silhouettes, especially between occluding hills, is useful (*silhouettes* in Section 3.2, Silhouettes).

—Water surfaces should reflect the environment (*water textures* in Section 3.3, Brushstroke Colors).

—Geometry should be emphasized by use of vertical exaggeration (*vertical exaggeration* in Section 3.4).

We computed the pupil diameters of the subjects at each frame of the video sequences. Lighting measurements made during video capture were used as input to our PLR model for simulating pupil behavior. The pupil diameters resulting from these simulations were then compared to the pupil diameters computed at individual video frames. Note that the simulated results are not expected to quantitatively match the observed ones, but rather be in qualitative agreement with observed behavior.

The videos were captured using a Cannon ELURA2 miniDV camcorder (NTSC, 720×576 pixels) with progressive scan, connected to a PC through a firewire connection. We kept the room's light dimmed so that the subjects' pupils could dilate naturally to some extent, but not so dark that we could not see the pupils in the individual video frames. Because of these constraints, we used two subjects (both males) with light eyes (a 24-year-old with green eyes, and a 26-year-old with blue eyes). For each frame, the pupil diameters were estimated from the set of dark pixels (pupil area P_{area}) inside a specified rectangle containing solely the subject's pupil and part of the iris (Figure 5). Given P_{area}, the pupil diameter was obtained (assuming the pupil is a circle) as $d = 2(\sqrt{P_{area}/\pi})$ pixels. The conversion from pixels to millimeters was performed considering a typical iris diameter of 12mm. According to our experience, computing the pupil diameter as described produces more accurate results than computing it as the number of pixels in the largest straight segment in the set of dark pixels (the pupil).

Since the video frames were captured at approximately 30Hz, in practice no variation is expected between the pupil diameters in neighbor frames under constant illumination, even in the presence of hippus. Thus, we estimated the average error in the computed pupil diameters to be approximately 0.1mm by computing the average difference between estimated pupil diameters for neighbor frames. Based on the video sequences, we set $S = 600$ (Equation (16)) for the two subjects in all experiments, as this value made their simulated constriction velocities approximate the ones in the video sequences. We empirically set the frequency of the two light sources used in our experiments to $R = 0.4$Hz, a value that made the latency estimated by Equation (1) approximate the latency observed in the video frames.

To evaluate the quality of our simulations, we performed experiments with both subjects using two different kinds of light sources to induce pupil constriction: a small flashlight and a 100-watt incandescent white light bulb. For light measurements, we used an LD-200 Instrutemp digital lux meter (precision ±3%, frequency 2 Hz).

6.4.1 *The Flashlight Experiments.* In these experiments, we used a light source to induce significant changes in the subjects' pupil diameters without introducing considerable changes in the lighting conditions of the environment. For this purpose, we used a small flashlight powered by a single AAA battery (1.5 Volt) kept at about 20cm from the subject's right eye and pointed at it. Given the small area illuminated by the flashlight as well as its reduced

power, the readings from the lux meter were very sensitive to even small changes in the relative position and orientation of the flashlight with respect to lux meter sensor. Thus, we decided to run two simulations using the recorded data: (1) considering the light intensity estimated using Equation (2), and (2) considering the readings from the lux meter. These two experiments are explained next.

In this experiment, we used the Moon and Spencer equation (Equation (2)) to solve for the light intensities during the on and off states of the flashlight, based on the measured pupil diameters (from the video). Since the Moon and Spencer function (curve C_m in Figure 3) represents the pupil behavior of an average individual, we estimated the on (off) light intensity as the average of the computed on (off) intensities for both subjects. Using this procedure, we obtained estimates of $10^{1.1}$ blondels when the flashlight was on, and $10^{-0.5}$ blondels when the flashlight was off. Given the average luminance value for the on (off) state and the corresponding pupil diameter for a given subject, we used Equation (19) to estimate the $r_{I_{on}}$ ($r_{I_{off}}$) index for that subject. The subject's final r_I index was computed as the average between his $r_{I_{on}}$ and $r_{I_{off}}$ indices. Using this procedure, we obtained $r_I = 0.4$ for the green-eye subject and $r_I = 0.03$ for the blue-eye subject.

Figure 6 shows the actual pupil diameter measurements performed on a frame-by-frame basis along 9-second-long sequences captured for each subject. The green "+" marks on top represent the measurements for the green-eye subject, while the blue "x" marks show the measurements of the blue-eye subject. This example illustrates the intersubject variability in terms of light sensitivity and shows the ability of our model to appropriately represent such individual differences. The vertical dotted lines delimit the intervals in which the flashlight was kept on and off for each subject. The solid and dashed lines represent the simulated results produced by our model for the green-eye and blue-eye subjects, respectively, and closely agree with the actual measured values. These curves were produced automatically from Equations (16) and (19), on top of which we added small random variations (hippus effect) as described in the previous section. The accompanying video shows side-by-side comparisons of our simulated results and videos captured for the two subjects.

6.4.1.1 *The second flashlight experiment.* In this experiment, we used the readings provided by the lux meter for the on and off states of the flashlight. These illuminance values were 350lux[1] and 90lux, respectively. One should recall that in such a setup, small changes in the position and orientation of the subject's head produce changes in the illuminance at the pupil. Therefore, these values are only approximations to the actual illuminance reaching each subject's lit eye. Given the illuminance values and the subjects' corresponding pupil diameters estimated from the video frames, we obtained the actual pupil's luminous flux (in lumens) at the two flashlight states, for each individual. These values were then converted to blondels according to the assumption described in Section 6.1. We then used Equations (16) and (19) to estimate their corresponding r_I indices (by averaging $r_{I_{on}}$ and $r_{I_{off}}$), obtaining $r_I = 0.54$ for the blue-eye subject and $r_I = 0.92$ for the green-eye subject. Figure 7 compares the actual pupil measurements (same as in Figure 6) with the results simulated by our model using the lux meter readings as input. The differences between the simulated curves shown in Figures 6 and 7 are primarily due to the added random noise (hippus).

---

[1]$1\ lux = 1\ lumen/m^2$.

6.4.2 *The 100-Watt Lightbulb Experiment.* For this experiment we used a more stable light source to induce pupil constriction: a spot with a 100-watt incandescent white lightbulb, kept at about one meter in front and one meter to the right of the subject's head. This setup allowed the subjects to remain comfortable with their eyes opened while the light was on.

We measured the environment light intensity during the on and off states by positioning the digital lux meter at approximately the same position and orientation as the subject's right eye. During the blue-eye subject experiment, we found the illuminance to be equal to 140 lux when the light was off and 315 lux when it was on. During the green-eye subject experiment, the readings were 91 and 540 lux, respectively. These differences resulted from a darker environment and a slight approximation of the green-eye subject to the light source. Again, we used the illuminance values and the subjects' corresponding pupil diameters (measured from the video) as input to Equations (16) and (19) to estimate their corresponding r_I indices (by averaging $r_{I_{on}}$ and $r_{I_{off}}$). We obtained $r_I = 0.9$ for the blue-eye subject and $r_I = 1.0$ for the green-eye subject.

Figure 8 (top) shows the actual pupil diameter measurements performed on a frame-by-frame basis along 56- and 50-second-long sequences captured for the blue-eye and for the green-eye subjects, respectively. The vertical lines delimit the intervals in which the light was kept on and off for each subject. The solid and dashed lines represent the simulated results produced automatically by our model (Equations 16 and 19) with and without hippus, respectively, and closely agree with the actual measurements. Figure 8 (bottom) shows zoomed versions of portions of the graphs shown on top, exhibiting off-on-off transitions.

One should note that the simulated results produced by our PLR model closely approximate the actual behaviors of the subjects' pupils in all three experiments, illustrating the effectiveness of our model. The differences in the r_I indices for a given subject among the experiments can be explained as follows.

—In the two flashlight experiments, the pupil diameters used for the on and off states were the same, but the illuminance values provided by Equation 2 and by the lux meter were different. The different indices simply reflect the different light sensitivities presented to our model as input.

—When comparing the 100-watt lightbulb and the flashlight experiments, both the lighting and the pupil sizes varied for the on and off states of the light sources. For instance, for the green-eye subject, the pupil diameters were approximately 4.3mm and 5.7mm for the on and off states of the flashlight, respectively (Figure 7). This resulted in an r_I index of 0.92. In the case of the 100-watt lightbulb experiment, these values were approximately 4.3mm and 6.0mm, respectively (Figure 8), with $r_I = 1.0$. These two indices are relatively close and reflect the difference in the maximum pupil diameters between the two experiments. The difference in the r_I indices for the blue-eye subject were considerably larger, from 0.54 to 0.9. Again, this can be explained by comparing the measured pupil diameters in the two experiments. These values went from approximately 3.2mm and 4.2mm in the on and off states of the flashlight (Figure 7) to 4.4mm and 5.2mm in the on and off states of the 100-watt lightbulb (Figure 8).

An important point to note is that by using an average of the estimated r_I indices for the on and off states of the light source, our model is capable of realistically simulating the pupil behavior of individuals with considerable differences in PLR responses under different and variable lighting conditions.

7. MODELING THE IRIS DEFORMATION

Although the iris is a well-known structure, there is no general agreement about a model of its behavior. He suggested that the collagen fibers are arranged in a series of parallel arcs, connecting the iris root with the pupil border, clockwise and counterclockwise in an angle of 90 degrees oriented by the center of the pupil. These fibers would be interwoven with other iris components, such as blood vessels. Based on Rohen's fiber arrangement, Wyatt proposed a 2D nonlinear model for iris deformation. Such a model has been validated on canine, porcine, and monkey irises, but so far not on human irises [Wyatt private communication].

Figure 9 (right) shows how the positions of the individually tracked iridal feature points changed along the dilation process. The trajectories of the points both on the pupillary and ciliary zones move on approximately radial paths. Although some imprecision in the exact location of the points might have resulted from the manual specification, most of the deviation from the radial paths result from the existence of blood vessels under the iris, and from crypts, and folds (the iris folds its tissue as a result of pupil dilation) that prevent iris points from always moving along radial lines. Such structures vary considerably among individuals but, according to our experience, their influence on the paths of the feature points usually has small magnitude (Figure 9 right). Therefore, as a first approximation, we can assume that the iris points move along straight lines in the radial directions. It is worth noting that Wyatt's 2D model does not take the influence of these structures into account either.

In order to find how fast the feature points moved, we computed the following measures during the dilation process: (1) the distance from the tracked feature point to the pupil center; (2) the distance from the tracked feature point to the pupil border; and (3) the ratio between the distance from the tracked point to the pupil border and the local width of the iridal disk (the distance from the pupil border to the external iris border measured along the radial segment passing through the feature point). One should recall that the pupil is not necessarily circular and that its center does not necessarily coincide with the center of the iris. While measurements (1) and (2) presented a pretty much linear behavior, the ratio represented by (3) was approximately constant for all feature points (Figure 10 right). The same behavior was observed in the irises of all five volunteers. Like the variations in the trajectories of the points shown in Figure 9 (right), the deviations from horizontal lines in Figure 10 (right) are caused by the subjects' iris structures, specially the iridal folds. Again, as a first approximation, the following ratio can be assumed constant for any iridal point p_i, for all values of pupil diameters:

$$\rho_i = \frac{\|p_i - c_i\|}{\|E_i - c_i\|}, \tag{20}$$

where p_i is a point on the iris disk, c_i and E_i are the points on the pupil border and on the iris outer circle, respectively, such that they are collinear to the radial segment passing through p_i. $\|.\|$ is the L^2 (Euclidean) norm. The invariance expressed by Equation 20 summarizes the observations illustrated in Figure 10 (right) and is the basis of our image-based model for iridal pattern deformation.

7.1 Animating the Deformed Iridal Patterns

As an approximation to the behaviors depicted in Figures 9 (right) and 10 (right), we use texture mapping to animate the iris deformation process. Note that this is a natural and efficient way of implementing the behavior modeled by Equation (20): as the pupil dilates/constricts, the iris ring is compressed/stretched, but the pa-

rameterization (in the $[0, 1] \times [0, 1]$ domain) of the points inside the ring remains the same. Thus, for animation purposes, we model the iris as a planar triangle-strip mesh on the disk defined by the two circles iris with a small pupil diameter as a texture. Texture coordinates map the border of the pupil to the inner circle of the mesh, and outer border of the iris to the mesh's outer circle. Currently, we tessellate the mesh creating a pair of triangles at every five degrees. The animation proceeds by computing the new pupil diameter D as a function of the incident lighting using Equation (19). We then reposition each vertex v_i, located on the inner circle of the mesh, at a distance $D/2$ along the radial line connecting the center of the pupil to v_i, while keeping their original texture coordinates unchanged. One should recall that the center of the pupil does not necessarily match the center of the iris, and thus, it is important to keep the coordinates of the center of the pupil. Figure 8 shows the renderings of an iris created using our models for different lighting conditions. Note that the patterns deform in a natural way. No light reflection on a corneal surface has been simulated, to avoid masking iris details.

8. DISCUSSION

We have implemented the proposed models and used them to render synthetic images of the human iris and pupil. The resulting animations are very convincing and run in real time. We have compared the images produced by our models with photographs and videos of real human irises. The results produced by our models are in qualitative agreement with observed behavior in humans.

In order to demonstrate the potential use of the proposed models in computer graphics, we built an application that renders a human head model in an environment illuminated by HDR cube maps (see accompanying video). The head model was obtained and its original irises were replaced by our textured triangle-strip model. The HDR images were obtained from Paul Debevec's web site and are used to approximate the environment's radiance. As the head looks at different parts of the environment, its pupil diameters adapt to the irradiance in the solid angle defined by its field of view, producing pleasing animation effects.

Accommodation and age affect the pupil diameter and iris color influences some PLR parameters, such as maximum pupil diameter, latency, and constriction velocity. These aspects are currently not taken into account by our model because of the lack of reliable data over a large range of lighting conditions. For instance, discuss the effect of age on the size of the pupil. Their study, however, only considered luminance values from 10^1 to 10^4 blondels, which corresponds to only about 30% of the luminance range used by our model. Currently, we model variations in pupil diameters for the same light stimulus using Equation 19, which can be used to simulate the age-related miosis effect reported by Winn. Also, since our model covers the entire range of valid pupil diameter values, it safely covers the pupillary sizes resulting from influence of attentional and other cognitive factors. Extending our model to handle other phenomena based on biophysical parameters is an interesting direction for future work.

No relief data representing the iris folds are used in the current version of the model, as it is done in the technique presented by. Also, no corneal refraction is used. Thus, at grazing angles, in addition to the distortion resulting from pupil dilation/constriction, one would perceive the projective distortion due to texture mapping. Relief information could be added to our model in a straightforward way, allowing some interesting shading effects such as projected shadows and self-occlusions.

We use a linear model for iridal pattern deformation even though the actual deformation is nonlinear. However, such nonlinearity contributes approximately only 1% of the diameter of a typical iris (12.0mm). Most of the nonlinear behavior seen in Figure 9 (right) and Figure 10 (right) is due to the interference of folds and blood vessels, which varies among individuals. To the best of our knowledge, no model in the literature takes those factors into account.

Many other factors affect pupil size, including particular states of mind, such as interest and curiosity, spectral sensitivity, respiratory and heart rate, and spatial patterns in the visual field. Taking all these aspects into account seems to be impractical due to their inherent complexity and limited supporting data. We should emphasize that PLR causes the single most noticeable involuntary movements of the pupil. As the graphs depicted in Figures 7 and 8 and the accompanying video show, our PLR model alone can produce predictable animations of the pupil dynamics.

9. CONCLUSION

We have presented new models for realistic renderings of the human iris and pupil. Our physiologically-based model of the pupil light reflex combines and extends theoretical results from the Mathematical Biology field with experimental data collected by several researchers. The resulting model is expressed in terms of a nonlinear delay-differential equation that describes the changes in the pupil diameter as function of the environment lighting. Our model is also original in the sense that it can simulate individual differences with respect to light sensitivity. As all parameters of our models were derived from experimental data, they correctly simulate the actual behavior of the human iris and pupil. They also produce high-fidelity appearance effects, which can be used to create real-time predictive animations of the pupil and iris under variable lighting conditions. We have validated our models through comparisons of our simulated results against videos and photographs captured from human irises. The quality of these simulations qualitatively matched the actual behaviors of human pupils and irises.

To the best of our knowledge, ours is the first physiologically-based model for simulating pupil light reflex presented in the graphics literature. It is also the first practical model (providing actual coefficient values) in the literature for simulating the dynamics of pupil and iris under variable lighting conditions, and the first integrated model in all of the literature to consider individual variability in pupil diameter using general equations for latency and velocity. Our image-based model for iridal pattern deformation is also the first model of its kind in the graphics literature.

10. TYPICAL REFERENCES IN NEW ACM REFERENCE FORMAT

A paginated journal article [Abril and Plant 2007], an enumerated journal article [Cohen et al. 2007], a reference to an entire issue [Cohen 1996], a monograph (whole book) [Kosiur 2001], a monograph/whole book in a series (see 2a in spec. document) [Harel 1979], a divisible-book such as an anthology or compilation [Editor 2007] followed by the same example, however we only output the series if the volume number is given [Editor 2008] (so Editor00a's series should NOT be present since it has no vol. no.), a chapter in a divisible book [Spector 1990], a chapter in a divisible book in a series [Douglass et al. 1998], a multi-volume work as book [Knuth 1997], an article in a proceedings (of a conference, symposium, workshop for example) (paginated proceedings article) [Andler 1979], a proceedings article with all possible elements [Smith

2010], an example of an enumerated proceedings article [Gundy et al. 2007], an informally published work [Harel 1978], a doctoral dissertation [Clarkson 1985], a master's thesis: [Anisi 2003], an online document / world wide web resource [Thornburg 2001], [Ablamowicz and Fauser 2007], [Poker-Edge.Com 2006], a video game (Case 1) [Obama 2008] and (Case 2) [Novak 2003] and [Lee 2005] and (Case 3) a patent [Scientist 2009], work accepted for publication [Rous 2008], 'YYYYb'-test for prolific author [Saeedi et al. 2010a] and [Saeedi et al. 2010b]. Other cites might contain 'duplicate' DOI and URLs (some SIAM articles) [Kirschmer and Voight 2010]. Boris / Barbara Beeton: multi-volume works as books [Hörmander 1985b] and [Hörmander 1985a].

APPENDIX

A. CLASSICAL MULTIDIMENSIONAL SCALING

Let D be an $n \times n$ matrix of pairwise distances. The matrix D is symmetric with a zero diagonal. We are interested in finding a $d \times n$ matrix X where each column $\boldsymbol{x}_i$ is the representation of the point i in R^d and $\mathrm{D}_{ij} = \|\boldsymbol{x}_i - \boldsymbol{x}_j\|_2$. Denote the inner product (or Gram matrix) for this set of points by $\mathrm{K} = \mathrm{X}^\top \mathrm{X}$.

K is an $n \times n$ symmetric positive semidefinite matrix. Let us now abuse notation and use D^2 to indicate the matrix of squared pairwise distances $\mathrm{K} = -\frac{1}{2}(\mathrm{I} - 11^\top)\mathrm{D}^2(\mathrm{I} - 11^\top)$. Here, I is the $n \times n$ identity matrix and 1 is the n-vector of all ones.

ACKNOWLEDGMENTS

REFERENCES

A. Ford and C. Raiciu and M. Handley and O. Bonaventure. current-year. TCP Extensions for Multipath Operation with Multiple Addresses. (current-year). http://tools.ietf.org/html/draft-ietf-mptcp-multiaddressed-09.

Rafal Ablamowicz and Bertfried Fauser. 2007. CLIFFORD: a Maple 11 Package for Clifford Algebra Computations, version 11. (2007). Retrieved February 28, 2008 from http://math.tntech.edu/rafal/cliff11/index.html

Patricia S. Abril and Robert Plant. 2007. The patent holder's dilemma: Buy, sell, or troll? *Commun. ACM* 50, 1 (Jan. 2007), 36–44. DOI:http://dx.doi.org/10.1145/1188913.1188915

Sten Andler. 1979. Predicate Path expressions. In *Proceedings of the 6th. ACM SIGACT-SIGPLAN symposium on Principles of Programming Languages (POPL '79)*. ACM Press, New York, NY, 226–236. DOI:http://dx.doi.org/10.1145/567752.567774

David A. Anisi. 2003. *Optimal Motion Control of a Ground Vehicle*. Master's thesis. Royal Institute of Technology (KTH), Stockholm, Sweden.

C. Paasch and S. Barre and J. Korkeaniemi and F. Duchene and G. Detal. current-year. MPTCP Linux Kernel Implementation. (current-year). http://mptcp.info.ucl.ac.be.

Kenneth L. Clarkson. 1985. *Algorithms for Closest-Point Problems (Computational Geometry)*. Ph.D. Dissertation. Stanford University, Palo Alto, CA. UMI Order Number: AAT 8506171.

Jacques Cohen (Ed.). 1996. Special Issue: Digital Libraries. *Commun. ACM* 39, 11 (Nov. 1996).

Sarah Cohen, Werner Nutt, and Yehoshua Sagic. 2007. Deciding equivalances among conjunctive aggregate queries. *J. ACM* 54, 2, Article 5 (April 2007), 50 pages. DOI:http://dx.doi.org/10.1145/1219092.1219093

D. DeCarlo and A. Santella. 2002. Stylization and abstraction of photographs. In *SIGGRAPH '02: Proceedings of the 29th annual conference on Computer graphics and interactive techniques*. ACM Press, New York, NY, USA, 769–776. DOI:http://dx.doi.org/10.1145/566570.566650

R. Dodge. 1900. Visual perception during eye movement. *Psychological Review* 7 (1900), 454–465.

R. Dodge and T. S. Cline. 1901. The angle velocity of eye movements. *Psychological Review* 8 (1901), 145–157.

Bruce P. Douglass, David Harel, and Mark B. Trakhtenbrot. 1998. Statecarts in use: structured analysis and object-orientation. In *Lectures on Embedded Systems*, Grzegorz Rozenberg and Frits W. Vaandrager (Eds.). Lecture Notes in Computer Science, Vol. 1494. Springer-Verlag, London, 368–394. DOI:http://dx.doi.org/10.1007/3-540-65193-4_29

A. T. Duchowski. 2002. A breadth-first survey of eye-tracking applications. *Behav Res Methods Instrum Comput* 34, 4 (Nov. 2002), 455–470.

Ian Editor (Ed.). 2007. *The title of book one* (1st. ed.). The name of the series one, Vol. 9. University of Chicago Press, Chicago. DOI:http://dx.doi.org/10.1007/3-540-09237-4

Ian Editor (Ed.). 2008. *The title of book two* (2nd. ed.). University of Chicago Press, Chicago, Chapter 100. DOI:http://dx.doi.org/10.1007/3-540-09237-4

D. A. Gajewski, A. Pearson, M. L. Mack, F. N. Bartlett III, and J. M. Henderson. 2005. *Lecture Notes in Computer Science*. Vol. 3368/2005. Springer Berlin - Heidelberg, Chapter Human Gaze Control in Real World Search, 83–99.

Google Inc. current-year. Google™ Image Search. (current-year). http://images.google.com/.

Matthew Van Gundy, Davide Balzarotti, and Giovanni Vigna. 2007. Catch me, if you can: Evading network signatures with web-based polymorphic worms. In *Proceedings of the first USENIX workshop on Offensive Technologies (WOOT '07)*. USENIX Association, Berkley, CA, Article 7, 9 pages.

David Harel. 1978. *LOGICS of Programs: AXIOMATICS and DESCRIPTIVE POWER*. MIT Research Lab Technical Report TR-200. Massachusetts Institute of Technology, Cambridge, MA.

David Harel. 1979. *First-Order Dynamic Logic*. Lecture Notes in Computer Science, Vol. 68. Springer-Verlag, New York, NY. DOI:http://dx.doi.org/10.1007/3-540-09237-4

Lars Hörmander. 1985a. *The analysis of linear partial differential operators. III*. Grundlehren der Mathematischen Wissenschaften [Fundamental Principles of Mathematical Sciences], Vol. 275. Springer-Verlag, Berlin, Germany. viii+525 pages. Pseudodifferential operators.

Lars Hörmander. 1985b. *The analysis of linear partial differential operators. IV*. Grundlehren der Mathematischen Wissenschaften [Fundamental Principles of Mathematical Sciences], Vol. 275. Springer-Verlag, Berlin, Germany. vii+352 pages. Fourier integral operators.

Markus Kirschmer and John Voight. 2010. Algorithmic Enumeration of Ideal Classes for Quaternion Orders. *SIAM J. Comput.* 39, 5 (Jan. 2010), 1714–1747. DOI:http://dx.doi.org/10.1137/080734467

Donald E. Knuth. 1997. *The Art of Computer Programming, Vol. 1: Fundamental Algorithms (3rd. ed.)*. Addison Wesley Longman Publishing Co., Inc.

David Kosiur. 2001. *Understanding Policy-Based Networking* (2nd. ed.). Wiley, New York, NY.

Newton Lee. 2005. Interview with Bill Kinder: January 13, 2005. Video, *Comput. Entertain.* 3, 1, Article 4 (Jan.-March 2005). `DOI:`http://dx.doi.org/10.1145/1057270.1057278

T. D. Nadeau and K. Gray. 2013. SDN: Software Defined Networks, Sebastopol. *O'Reilly Media* (2013).

Dave Novak. 2003. Solder man. Video. In *ACM SIGGRAPH 2003 Video Review on Animation theater Program: Part I - Vol. 145 (July 27–27, 2003)*. ACM Press, New York, NY, 4. `DOI:`http://dx.doi.org/99.9999/woot07-S422

Barack Obama. 2008. A more perfect union. Video. (5 March 2008). Retrieved March 21, 2008 from http://video.google.com/videoplay?docid=6528042696351994555

Poker-Edge.Com. 2006. Stats and Analysis. (March 2006). Retrieved June 7, 2006 from http://www.poker-edge.com/stats.php

C. Raiciu, C. Paasch, S. Barre, A. Ford, M. Honda, F. Duchene, O. Bonaventure, and M. Handley. 2012. How Hard Can It Be? Designing and Implementing a Deployable Multipath TCP. *USENIX Symposium of Networked Systems Design and Implementation (NSDI12)* (2012).

Bernard Rous. 2008. The Enabling of Digital Libraries. *Digital Libraries* 12, 3, Article 5 (July 2008). To appear.

Mehdi Saeedi, Morteza Saheb Zamani, and Mehdi Sedighi. 2010a. A library-based synthesis methodology for reversible logic. *Microelectron. J.* 41, 4 (April 2010), 185–194.

Mehdi Saeedi, Morteza Saheb Zamani, Mehdi Sedighi, and Zahra Sasanian. 2010b. Synthesis of Reversible Circuit Using Cycle-Based Approach. *J. Emerg. Technol. Comput. Syst.* 6, 4 (Dec. 2010).

Joseph Scientist. 2009. The fountain of youth. (Aug. 2009). Patent No. 12345, Filed July 1st., 2008, Issued Aug. 9th., 2009.

Stan W. Smith. 2010. An experiment in bibliographic mark-up: Parsing metadata for XML export. In *Proceedings of the 3rd. annual workshop on Librarians and Computers (LAC '10)*, Reginald N. Smythe and Alexander Noble (Eds.), Vol. 3. Paparazzi Press, Milan Italy, 422–431. `DOI:`http://dx.doi.org/99.9999/woot07-S422

Asad Z. Spector. 1990. Achieving application requirements. In *Distributed Systems* (2nd. ed.), Sape Mullender (Ed.). ACM Press, New York, NY, 19–33. `DOI:`http://dx.doi.org/10.1145/90417.90738

Harry Thornburg. 2001. Introduction to Bayesian Statistics. (March 2001). Retrieved March 2, 2005 from http://ccrma.stanford.edu/~jos/bayes/bayes.html